



Article

Estimation of Hydrogeological Parameters by Using Pumping, Laboratory Data, Surface Resistivity and Thiessen Technique in Lower Bari Doab (Indus Basin), Pakistan

Gulraiz Akhter^{1,2,*} , Yonggang Ge^{3,4,*} , Muhammad Hasan^{5,6,7}  and Yanjun Shang^{5,6,7} ¹ China-Pakistan Joint Research Center on Earth Sciences, CAS-HEC, Islamabad 45320, Pakistan² Department of Earth Sciences, Quaid-i-Azam University, Islamabad 45320, Pakistan³ Institute of Mountain Hazards and Environment, Chinese Academy of Sciences, Chengdu 610041, China⁴ Key Laboratory of Mountain Hazards and Earth Surface Processes, Chinese Academy of Sciences, Chengdu 610041, China⁵ Key Laboratory of Shale Gas and Geoenvironment, Institute of Geology and Geophysics, Chinese Academy of Sciences, Beijing 100029, China; hasan.mjiinnww@gmail.com (M.H.); jun94@mail.iggcas.ac.cn (Y.S.)⁶ Innovation Academy for Earth Science, Chinese Academy of Sciences, Beijing 100029, China⁷ College of Earth and Planetary Sciences, University of Chinese Academy of Sciences, Beijing 100049, China

* Correspondence: agulraiz@qau.edu.pk (G.A.); gyg@imde.ac.cn (Y.G.)

Abstract: Determination of hydrological properties of the aquifer is of fundamental importance in hydrogeological and geotechnical studies. An attempt has been made to refine the hydraulic conductivity values computed from the pumping test by utilizing the hydraulic values computed in the laboratory. This study uses hydraulic conductivity computed in the laboratory of rock samples, pumping test data in conjunction with the empirical equations, and vertical electric sounding (VES) to determine the hydraulic properties of Lower Bari Doab (LBD) in the Indus Basin of Pakistan. The utilized dataset comprises pumping test results (K_{pump}) from 17 water wells, hydraulic conductivity values (K_{lab}) of different grain size subsurface lithologies, and 50 VES stations. To this end, the investigated area is divided into 17 polygons by using the Thiessen technique, and equal distribution/weight of conductivities values is assigned to 17 polygons (one polygon around each water well where pumping test is conducted). The true resistivity ranging from 20–90 ohm-m along with an average thickness of the aquifer is computed using the VES data for each polygon. A novel approach has been developed to estimate the hydraulic conductivity of the aquifer by combining laboratory data and pumping test which is used to compute the other hydraulic properties. The calculated hydraulic conductivity, transmissivity, and tortuosity values of the aquifer range from 4.4 to 85.6 m/day, 674 to 8986 m²/day, and 13 to 20, respectively. The porosity ranges from 32 to 45% and the formation factor values fall in the range 4 to 12. Higher hydraulic conductivities were encountered in the southern portion of the area near the junction of the rivers, and it increases with an increase in porosity. The aquifer having $T > 5700$ m²/day and $K > 40$ m/day, yields a large quantity of water whereas the portion of an aquifer with $T < 1100$ m²/day and $K < 13$ m/day are comparatively low yield aquifer. The results of the resistivity method show that the subsurface geological material, as depicted from true resistivity, is composed of layers of sand, clay, and silt mixed with gravel/sand. This study improves the understanding of the aquifer and will help in the development and management of groundwater resources in the area including the prediction of future behavior of the aquifer.

Keywords: geophysical method; hydraulic conductivity; transmissivity; porosity; formation factor



Citation: Akhter, G.; Ge, Y.; Hasan, M.; Shang, Y. Estimation of Hydrogeological Parameters by Using Pumping, Laboratory Data, Surface Resistivity and Thiessen Technique in Lower Bari Doab (Indus Basin), Pakistan. *Appl. Sci.* **2022**, *12*, 3055. <https://doi.org/10.3390/app12063055>

Academic Editor: Ty P. A. Ferré

Received: 17 January 2022

Accepted: 10 March 2022

Published: 17 March 2022

Publisher's Note: MDPI stays neutral with regard to jurisdictional claims in published maps and institutional affiliations.



Copyright: © 2022 by the authors. Licensee MDPI, Basel, Switzerland. This article is an open access article distributed under the terms and conditions of the Creative Commons Attribution (CC BY) license (<https://creativecommons.org/licenses/by/4.0/>).

1. Introduction

The Indus Basin of Pakistan is the main source of water supply in Pakistan for different purposes, such as agricultural, commercial, and residential use. The Indus Basin groundwater aquifer in Pakistan holds at least 80 times the water stored in the country's three

largest dams (Tarbela Dam, Mangla Dam, and Mirani Dam) but is under severe pressure due to overexploitation that continues to occur due to the rapidly increasing population that has outpaced aquifer recharge. In 2020, Pakistan faced a huge groundwater crisis due to large-scale extraction from the aquifer. About 62 billion m³ of water is annually drawn from the aquifer from the Indus Basin which is about 1/3rd of the total annual water withdrawal in Pakistan [1]. Huge pumpage has resulted in a rapid decline in water level and as a result, groundwater availability and quality have substantially deteriorated [2–5]. The rapid installation of tube-wells without any geotechnical or geophysical investigation has lowered the groundwater level and has caused the salinity issue [6–10]. In the past, it was reported [11] a rise of more than 0.2 m per year, and in the Bahawalpur area (adjacent to Lower Bari Doab), the rate was nearly 0.4572 m per year [12]. However, in recent years, the trend has reversed [13] showed a decline of 15 m in the water table of the Upper Bari Doab since 1960. Mashadi and Mohammad [14] reported average change in the water table for the last several decades, the rates are shown in Table 1. It was found [15] that the yearly decline had increased to 2 to 3 m. The uncontrolled withdrawals have put the aquifer under stress by causing an imbalance between recharge and abstraction. In addition, increasing population, unconstrained pumping for agricultural needs, and climate change have disturbed the balance between water demand and supply. If groundwater depletion continues then the upper portion of the aquifer might run dry in the near future.

Table 1. Water table decline in the Upper Bari Doab area.

Period	Rate of Decline (m/Year)
1960–1967	0.2987
1967–1973	0.5486
1973–1980	0.6004
1980–2000	0.6492

Aquifer depletion can be arrested with better understanding and proper utilization of aquifer which in turn requires detailed groundwater profiling. Water flow and storage depend on the hydraulic properties of the aquifers and affect the timing, locations, and depletion of the aquifer which is important for hydrogeologists and policymakers to formulate appropriate management strategies and implementation of relevant interventions required. For this purpose, it is essential to know the accurate hydraulic properties of the aquifer [16]. Grain size, lithology, and geomorphic nature of the deposited sediments are important agents for the development of clastic fluvial aquifers and their hydraulic characteristics [17,18]. Depending on the origin, transporting agent, and distance from the source to depositional place, the sediments may vary in size from very coarse alluvial fan gravels and channel deposits. The depression fill deposits act as an aquifer with high hydraulic conductivity, whereas fine lacustrine clays have low hydraulic conductivity. For modeling purposes, hydraulic conductivity plays an important role in determining the flow through pores. It is also used for designing retention ponds, roadbeds, and any system designed to capture runoff. Hence, the prediction of water mobility within the aquifer needs accurate values of hydraulic parameters. Being an underground resource, the measurement, monitoring, and management of groundwater are more difficult than surface water. Using hydraulic properties, computer software such as Modflow, Visual MODFLOW, Feeflow, etc, estimate the rates, locations, and timing of streamflow depletion in response to groundwater pumping. Researchers have used various techniques including empirical equations developed for the particular area using surface resistivity methods and pumping to estimate aquifer potential and hydraulic properties [19–24].

Hydraulic properties of an aquifer are conventionally determined using either rock samples or pumping test results. Rock samples are taken from different depths and locations and analyzed in the laboratory which is costly and is seldom available. On the other hand, a pumping test yields information and cannot capture aquifer heterogeneity. The purpose

of this study is to provide the spatial distribution pattern of hydraulic properties of the aquifer in the Lower Bari Doab (LBD) in the Punjab Province.

The Lower Bari Doab (Figure 1) is an important part of the Upper Indus Basin. This study provides the characterization of hydraulic properties and is fundamental for the assessment of the future availability of groundwater resources and management. These hydraulic properties—including lithology, micro-fractures, conductivity, porosity, and permeability of the strata [25] can control the aquifer and thus, are mandatory for the development and management of the aquifer in an area. The results from this study would provide useful information for groundwater modeling that will lead to improved aquifer management.

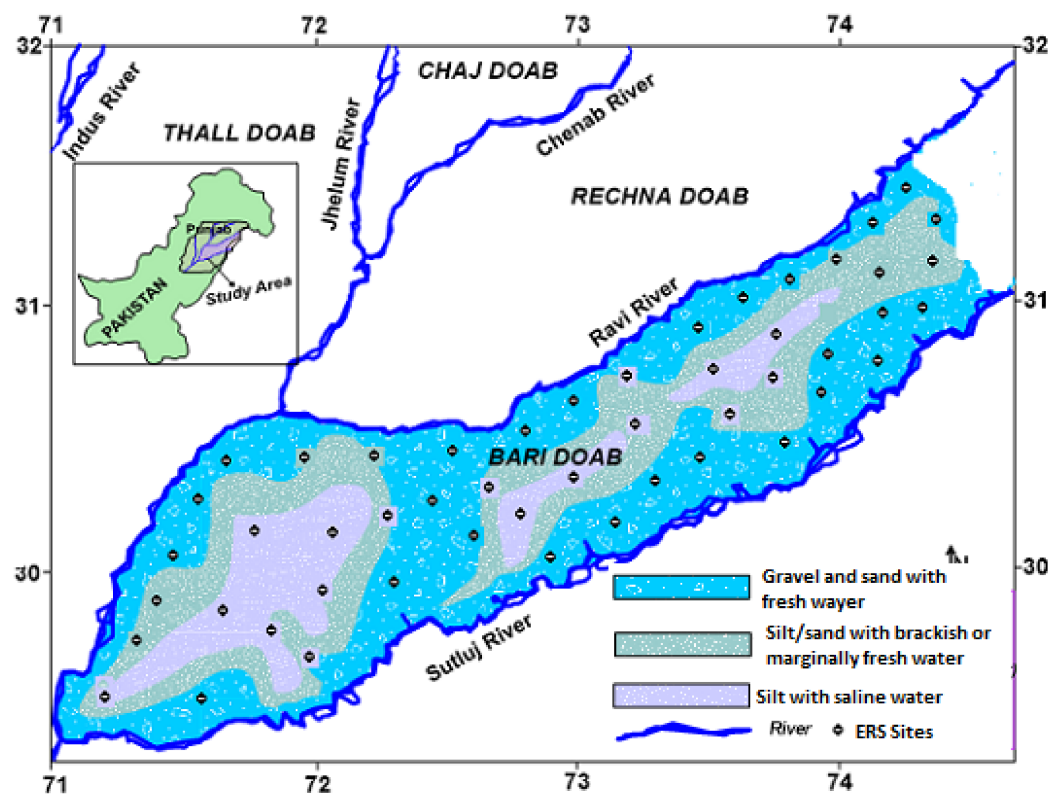


Figure 1. Hydrogeological map along with location Of ERS sites of Bari Doab (after [10]).

A novel approach to finding hydraulic properties of the aquifer by combining laboratory data and pumping test results for estimating hydraulic conductivity surrounding to pumping well has been introduced. The data obtained from the pumping test is refined using laboratory data of different depths which is then used to create zonations and in turn calculate hydraulic properties.

2. Materials and Methodology

Location of the study area: Indus Basin of Pakistan is subdivided into Upper and Lower Indus Basin. Upper Indus Basin consists of four hydrological units, locally known as Thal, Chaj, Rachna, and Bari Doab (Figure 1). Doab is the tract of land between two rivers. Upper Indus Basin is a well-transmissive and continuous unconfined aquifer where lithology varies from coarse sand to sandy loam with clay lenses [26]. The study area Lower Bari Doab (LBD) is bounded by Ravi and Chenab rivers in the northwest and west, respectively, and by the Sutlej River in the southeast. On the eastern side, it shares a border of nearly 80.5 km with India. The total area of the doab is nearly 19,600 km². It is about 402 km in length from the border to the confluence of Chenab and Sutlej Rivers and the average width is nearly 96.5 km [27]. LBD is located between latitude 29°30' to 31°45' N and longitude 71° to 74°45' E (Figure 1). The northeastern boundary of Bari Doab lies near

the foothills of the Himalayan range and almost coincides with the Lahore district. LBD is a part of the Indus Basin Irrigation System and comprises a network of canals [28].

Climate: Agriculture is the principal occupation in Lower Bari Doab. There are two seasons termed Kharif and Rabi. The Kharif season includes the monsoon months starting from 15 July to 15 September and the Rabi season is the relatively dry winter season from 15 October to 15 April. The climate is arid to semi-arid, and the mean annual precipitation ranges from 102 mm in the south to 508 mm in the north. Two-thirds of this precipitation occurs in the four summer months. Maximum temperature ranges from about 20 °C in December and January to about 41 °C in May and June.

Hydrogeology: Lower Bari Doab is a part of the Indo-Gangetic Plain and is covered by Quaternary alluvium, which presumably overlies semi-consolidated tertiary rocks or metamorphic and igneous rocks of Precambrian age [29]. Several deep test holes ranging from 243.83 to 396.22 m depth were drilled to determine the thickness of the alluvium and the depth of the bedrock. In these test drills, the bedrock was encountered in only three holes at 381.59, 311.19, and 282.84 m in the northeastern part of the Bari Doab [29]. Therefore, in the Lower Bari Doab area, the total thickness of the Quaternary alluvium and the distribution of tertiary and older rocks were not found [30].

The subsurface lithology consists of mainly sand encountered in test holes and water wells showed the water-bearing characteristic of the alluvial deposits, that form the aquifer of the Bari Doab. A comparative study of the lithological logs provided a fairly good idea about the texture and structure of the heterogeneous alluvium to the depth of 183 m. The subsurface lithologies inferred in the Quaternary alluvial complex consisted of clay, sandy silt, fine sand, fine-to-medium sand, medium-to-coarse sand, coarse sand, and gravel. The alluvial material covering the study area formed part of the extensive heterogeneous and isotropic unconfined aquifer underlying the Indus Basin and was believed to be more than 304.79 m thick. Geological evidence also indicated that the aquifer is unconfined [31]. The aquifer yield varies from 100 to 300 m³/h in Bari Doab [10] (Figure 1).

Electrical Resistivity Survey: The geoelectrical method measures the distribution of the subsurface resistivity which is a physical property depending on the characteristics of the materials [32]. The principle of the electrical resistivity method is based upon injection/passage of electric currents into the ground for the discovery of electrical features of the materials buried in the ground [33]. This method is quick and cost-effective and has proven more successful for describing subsurface lithological and hydrogeological features [34,35] and groundwater conditions and subsurface layers [36,37]. This method is also used to estimate the hydrological parameters of the aquifer. Many researchers have evaluated aquifer parameters using the resistivity method [38–40]. This method has been utilized for indirect estimation of K and T, reducing the need to drill boreholes that were used for pumping tests [41–43].

Electrical resistivity survey is a practical application of Ohm's law, as shown in Equation (1), to map the subsurface changes in earth resistivity and correlate them with the hidden geological formations.

$$R \propto \Delta V/I \dots \text{ or } \dots R = K \times (\Delta V/I) \quad (1)$$

where R is apparent resistivity (ohmmeter); ΔV = Voltage (potential drop) measured in milli-volt; I = current (milli-ampere); and K = Schlumberger constant of proportionality.

The apparent resistivity depends on the injected current I, measured potential V, and the geometric factor K [33,44]. Current injected into the subsurface is affected by many features of the strata such as priority organic components, minerals such as silt, clay, packing of void spaces, fluid presence, etc. in subsurface strata [45]. This method is used profitably to determine qualitatively the type of water-bearing formation, e.g., sand, sandstone, gravel, boulder provided conditions are favorable and not complicated by abrupt lateral changes in lithology. In resistivity surveys, a commuted direct current is introduced into the ground via two electrodes (A & B). The potential difference is measured between the second pair of electrodes (M & N). The four electrodes are arranged in any of several possible patterns. The

current and potential measurements are then used to calculate apparent resistivity values. The layout of current and potential electrodes is shown in Figure 2. For data acquisition, Schlumberger electrode configuration is applied which is the most widely used in the world for conducting electrical resistivity surveys. The electrodes are placed along a straight line on the earth's surface by satisfying the condition given in Equation (2).

$$AB \leq 5 MN \quad (2)$$

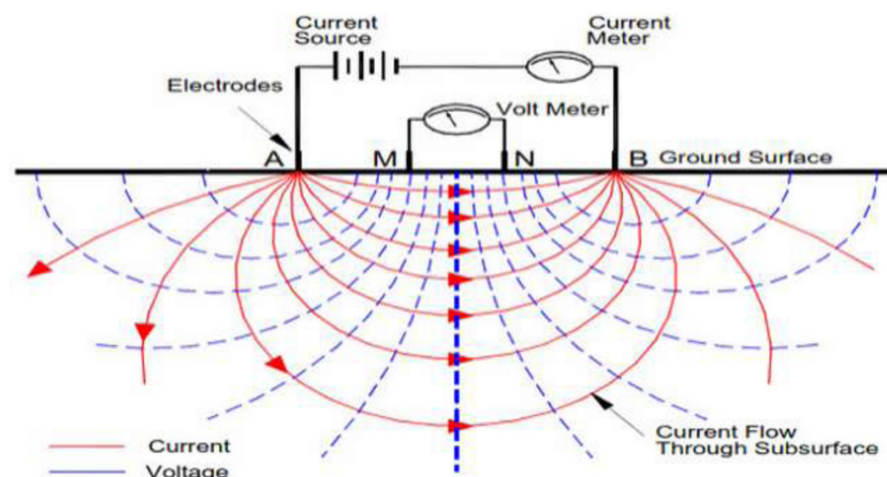


Figure 2. Schematic illustration of the VES technique and electrode arrangement for Schlumberger configuration.

In this study, a total number of 50 VES probes were conducted to map the subsurface lithologies. Some of the points near the water wells were used for calibration purposes. The geoelectric parameters of VES-30 were correlated with lithologic data from 1 of 17 water wells and interpreted the lithologies of VES-30 were shown in Figure 3. IXID software is used to calculate the true resistivity together with the thickness of all possible geoelectric layers encountered in the depth of investigation. The modeled (true) resistivities of VES points reflect the subsurface lithologies up to a depth of penetration and hence provide information on the subsurface geology of the area. The resistivity of the rock is controlled by various factors such as water and clay content, porosity, temperature, and fault [46]. The subsurface lithologies are interpreted on a local basis relating to the nature and characteristics of the rocks existing in that area [46,47].

The average resistivity of all materials calculated in the field known as the apparent resistivity of 50 probes was analyzed for the estimation of aquifer quality. The inverse iterative technique was applied to obtain true resistivity and layer thickness for different sub-surface layers using IXID software. Factors, such as porosity, temperature, clay content, and water content, affect the actual resistivity of the material [46]. The nature and characteristics of the rock mass existing in the area play an important role to interpret the sub-surface lithologies [48]. A relation can be established between aquifer lithology and the resistivity to map the geometry of sub-surface layers, provided that the rock mass is correlated with resistivity ranges [49] (Rucker et al., 2011). Resistivity method is also used to classify freshwater and saltwater horizons, groundwater quality [50–53] and demarcate of fresh and saline water boundary [54,55].

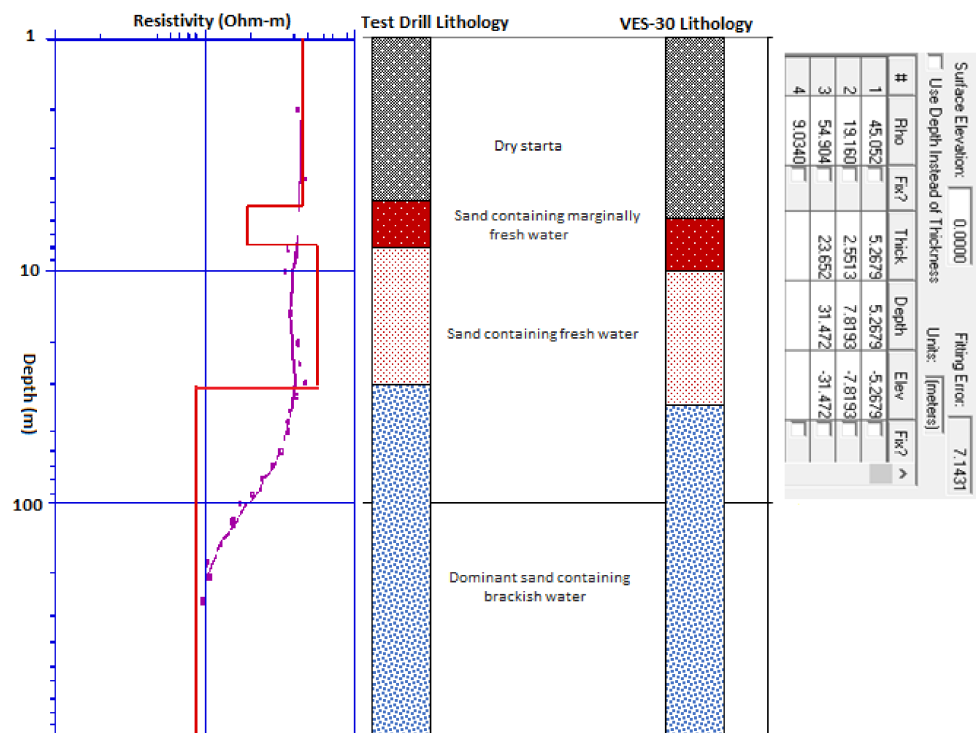


Figure 3. Correlation between sounding curve-30 with test drill lithology along with modeled parameters.

Based on the calibrated results (Figure 3), between resistivity modeled curve-30 and borehole lithology, a standard correlation of layers was prepared separately for lithologies listed in Table 2. This standardized correlation was then applied to all VES data points. The computed resistivity ranged from 20 to 90 Ω-m, indicating aquifer for 17 polygons having fresh to saline water in the study area is presented in Table 2.

Table 2. True resistivity and aquifer lithology calibration in Lower Bari Doab, Pakistan.

Resistivity (ohm-m)	Lithology
Less than 20	Silt containing saline water; Dominant sand containing brackish water
20–40	Sand containing marginally fresh water
40–55	Sand containing fresh water
Greater than 55	Mixture of sand and minor gravel containing fresh water

Pumping Test: Depending on the nature/type of the aquifer, various techniques are applied to pumping data (time drawdown vs. time) to find the hydraulic parameters of the aquifer. These parameters are important for the prediction of the future availability of groundwater reserves [23,56]. Aquifer parameters including hydraulic conductivity, transmissivity, and storativity are commonly applied in groundwater modeling [40,57,58] and these parameters are also estimated using the hydro-geophysical technique [16,56,59,60]. Permeability and formation factor can be estimated using empirical correlation [39,61]. The method proposed [62] for estimating the transmissibility and storability of aquifers using specific well capacity. Aquifer characteristics and electrical parameters of the geoelectrical layers have been studied by many researchers [9,63–66].

Hydraulic conductivity can be considered the basic parameter that describes the hydrogeology of the aquifer of any area and the main aquifer parameter to estimate the characteristics of the aquifer. It is more effectively estimated using geological information

extracted from drilled wells or test hole wells. It governs, along with other parameters, the flow of fluids and the migration of contaminants in the subsurface lithologies. Hydraulic conductivity is a measure of how easily water can pass through soil or rock: high values indicate permeable material through which water can pass easily and vice versa.

The Lower Bari Doab (LBD) is part of the Indus Basin is very important for the characterization of hydraulic properties, fundamental for the assessment of the future availability of groundwater resources and precise management.

To model the behavior of hydraulic conductivity in the aquifer, a grid consisting of 66 columns by 26 rows is overlaid on the area with a spacing of 5000 m, both in X- and Y-directions. For this purpose, test holes and water wells are used which had been drilled during different exploration stages by WAPDA. The pumping test data and the hydraulic characteristics of these water wells were also studied [31,67,68].

In addition to the pumping test data and subsequent results, laboratory hydraulic conductivity (K_{lab}) comprising different subsurface materials from different depth intervals was also available from test holes located in the study area. Although not all intervals were sampled, a lithological description was available for different depths. A value of K_{lab} from an identical lithology was assigned to intervals for which a measured hydraulic conductivity was not available. The values of the laboratory conductivity were lower than the conductivity obtained from the pumping test analysis data due to the obvious reason that the samples obtained from different depths were disturbed and their physical properties (porosity, packing, grain orientation) were also variable. The difference between the K_{lab} and pumping test hydraulic conductivity values (K_{pump}) was adjusted to K_{lab} by devising a mechanism [69,70] to evaluate the conductivity (K). By taking the geometric mean, the conductivity values (K_{lab}) beneath each test hole were averaged out, and thus a single value termed, individual laboratory conductivity, was assigned to an aquifer for an individual polygon. A flowchart describing the workflow methodology to establish the hydraulic conductivities zones of the LBD area is shown in Figure 4.

Lab Data: Based on the similarities and/or slight differences between the values of K_{lab} followed by the 2-directional geological distribution, zones comprising equal values were formulated for an aquifer. By taking the geometric mean of the values computed of samples representing different depths, a single value of a test hole is assigned. If the difference between the hydraulic conductivity values computed in a laboratory for test holes is less or equal to 1×10^{-7} m/s, then that group of values has been assigned a zone. If the difference is more than 1×10^{-7} m/s, then that cluster of values is assigned a new zone and so on. The zonation of aquifer K_{lab} is shown in Figure 5.

A similar methodology is used for the conductivities of pumping test analysis that leads to the generation of different zones having a single value of K_{pump} as shown in Figure 6. The difference between the K_{lab} and K_{pump} was obtained and added this difference (K_{diff}) to the individual laboratory conductivities, previously evaluated, and on this basis, new conductivities were obtained for the model termed " K_{model} ". The zones are made for the K_{model} values for the aquifer are shown in Figure 7.

To establish an equal distribution and/or weight of conductivity values, the K_{model} around the water wells and Thiessen Polygon Method [71] were used. This method has been globally used in meteorology and hydrology for guessing areas from point observations [72]. This technique [73] was also utilized for estimating hydraulic conductivity in the surrounding area (Thal Doab) by developing various zone to model the subsurface aquifer. This methodology is applied in the present study by replacing point observation into a water well where the pumping test is performed, a polygon is developed around the well and hydraulic conductivity is estimated within that polygon. The study area was divided into 17 polygons. The number of conductivity values that fall within each polygon was increased by the K_{diff} obtained from the conductivities of K_{lab} and K_{pump} at the test hole

location. The area lies on the boundary of polygons and was assigned a single value by taking the geometric mean of the values of those polygons established around water wells are unique representations of their kind. The methodology for obtaining the final value of conductivity (K) (Geometric Mean of K_{model} values) and its distribution using polygons are shown in Table 3 and Figure 8. The final computed values of hydraulic conductivities estimated by using this technique ranging from 4 m per day to 85 m per day are in close agreement with already computed values calculated by Akhter and Hasan in 2016 [58] of the area that falls within the Lower Bari Doab. They used Aquifer Test Pro software for the aquifer system by using a pumping test for 7 wells and estimated the hydraulic values ranging from 15.9 to 60.9 m per day. In addition, the results of the electrical resistivity survey showed that sand is the dominant subsurface lithology (Table 2). The values of hydraulic conductivities of the interpreted lithology closely matched with the values available in the literature [74–76]. Similarly, the other properties like porosity and transmissivity computed with the help of mathematical relation by using the current refined values of hydraulic conductivities are fall within the range of published literature.

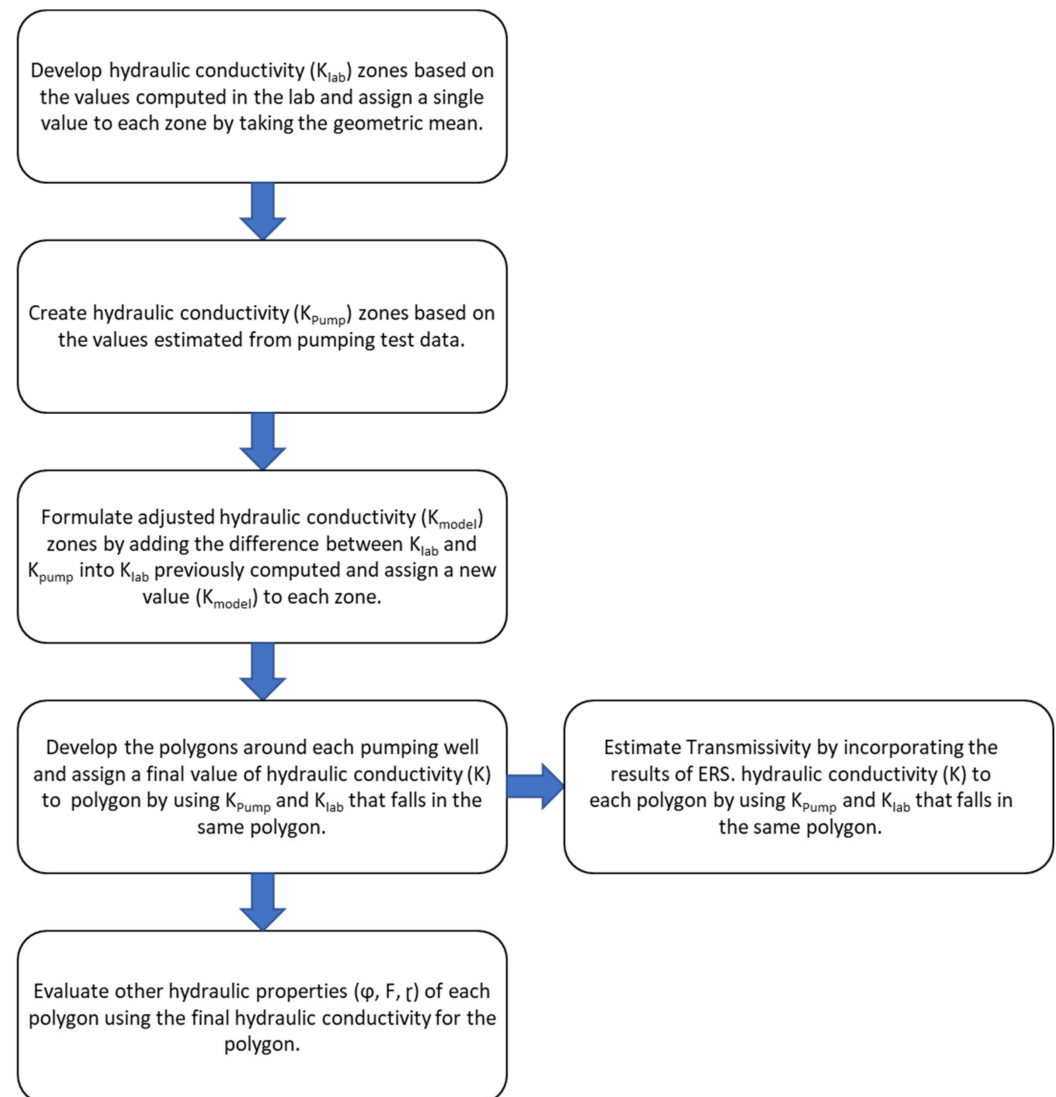


Figure 4. Workflow to establish the hydraulic conductivities zones and estimate the other hydraulic properties.

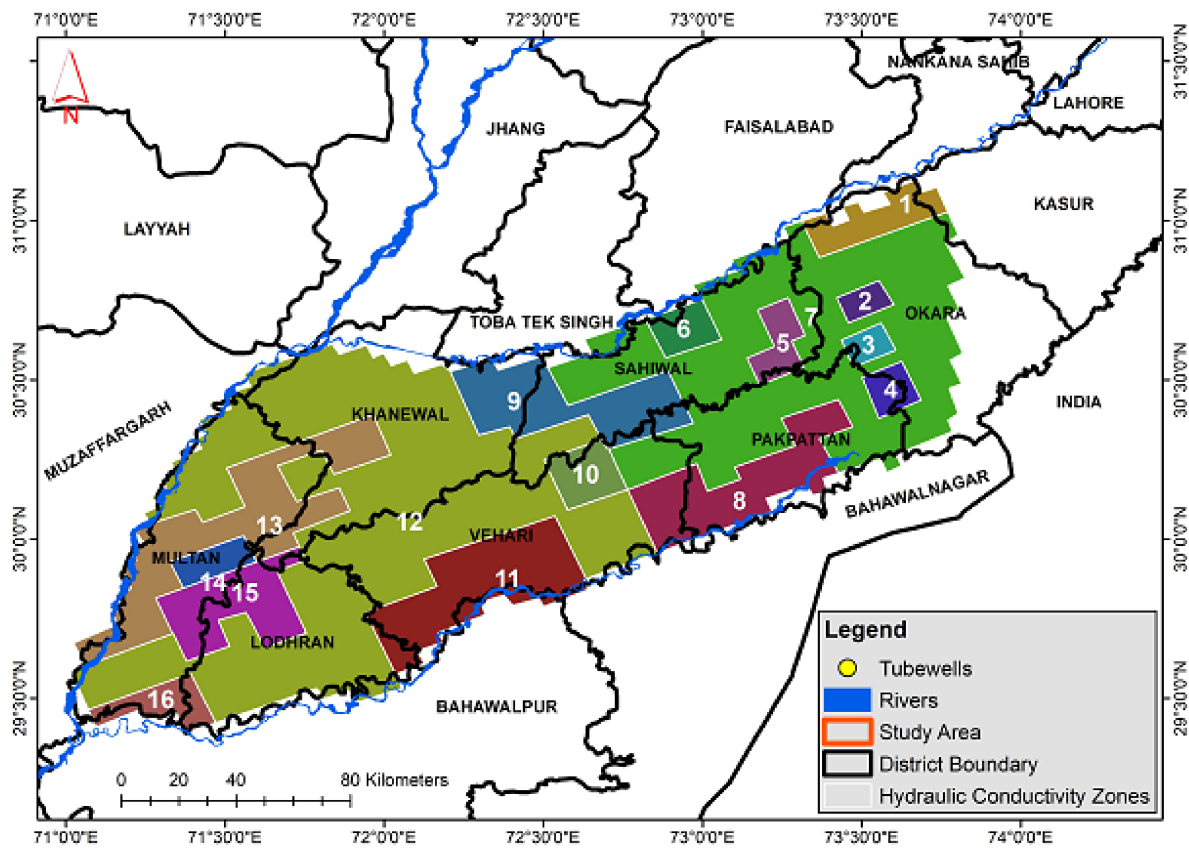


Figure 5. Zonation of hydraulic conductivity (K_{Lab}) of the aquifer based on laboratory analysis.

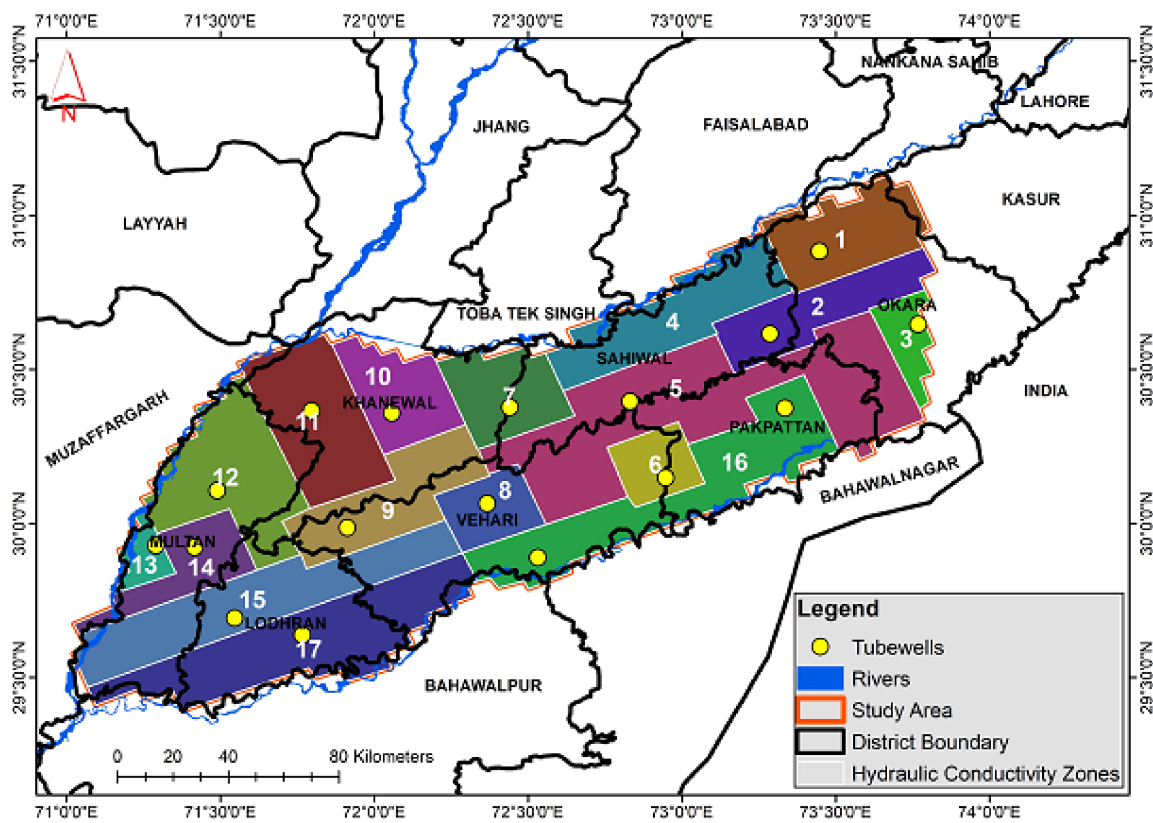


Figure 6. Zonation of hydraulic conductivity (K_{pump}) of the aquifer based on pumping test data.

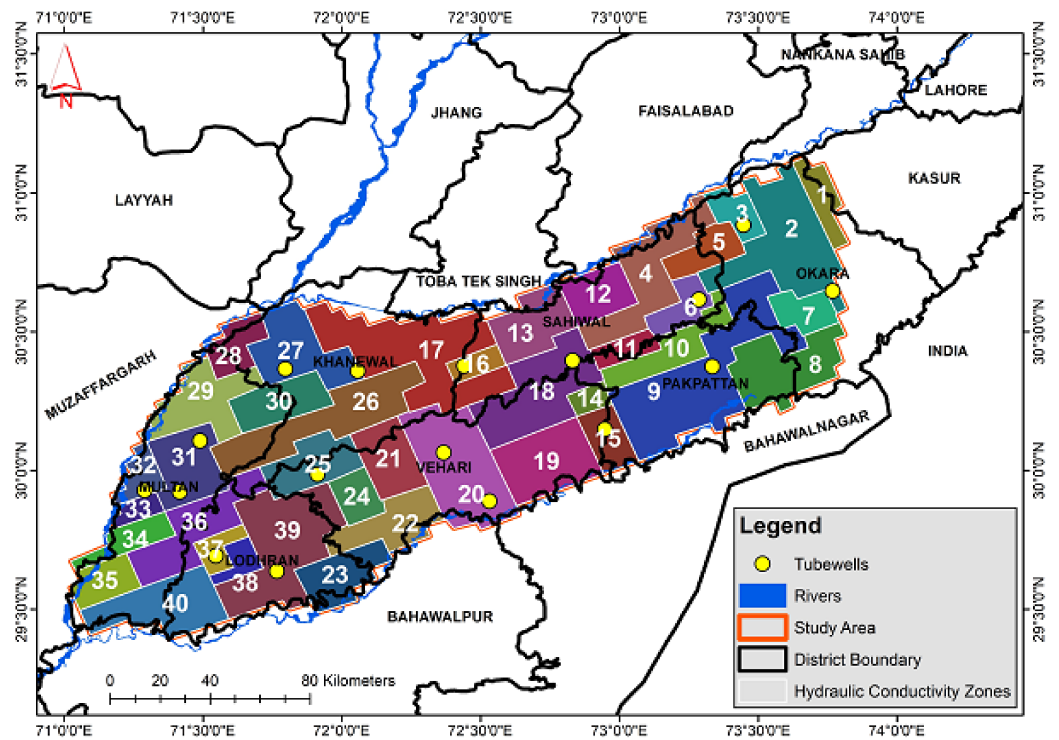


Figure 7. Zonation of adjusted hydraulic conductivity (K_{model}) of the aquifer.

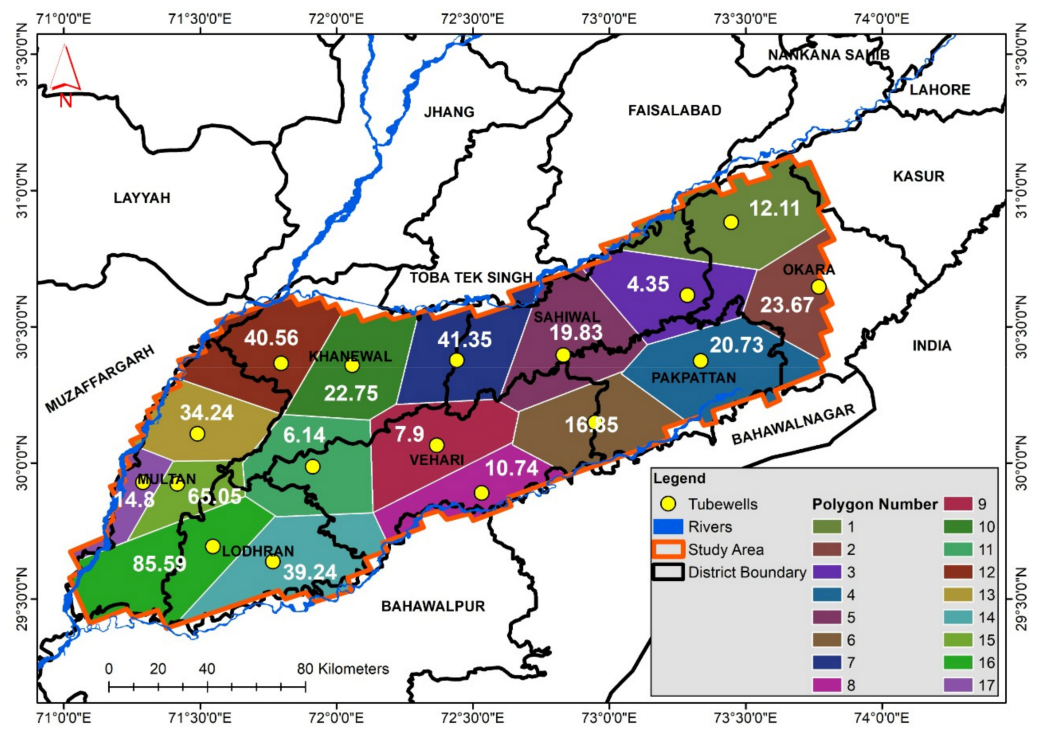


Figure 8. Distribution of final value of hydraulic conductivity K (m/day) indicated in polygons.

Table 3. Methodology used for computing the final value of hydraulic conductivity.

Polygon #	Log K_{pump} (m/s)	Log K_{lab} (m/s)	$K_{diff} =$ Log $K_{pump} -$ Log K_{lab} (m/s)	Test Hole K_{lab} (m/s)	Log K_{lab} (m/s)	Log $K_{model} = K_{diff}$ + Log K_{lab} (m/s)	K_{model} (m/s)	Geometric Mean K (m/day)
1	−2.5430	−5.2940	2.7510	3.20×10^{-7}	−6.49	−3.74	1.80×10^{-4}	12.11
				3.84×10^{-7}	−6.42	−3.66	2.16×10^{-4}	
				2.90×10^{-7}	−6.54	−3.79	1.63×10^{-4}	
				1.77×10^{-8}	−7.75	−5.00	1.00×10^{-5}	
				1.49×10^{-7}	−6.83	−4.07	8.41×10^{-5}	
				8.41×10^{-7}	−6.08	−3.32	4.75×10^{-4}	
				1.83×10^{-7}	−6.74	−3.99	1.03×10^{-4}	
2	−3.0160	−5.4610	2.4450	1.01×10^{-6}	−6.00	−3.25	5.67×10^{-4}	23.67
				7.68×10^{-7}	−6.11	−3.67	2.14×10^{-4}	
				1.77×10^{-6}	−5.75	−3.31	4.94×10^{-4}	
				9.97×10^{-7}	−6.00	−3.56	2.78×10^{-4}	
				3.78×10^{-6}	−5.42	−2.98	1.05×10^{-3}	
3	−2.3450	−4.7720	2.4270	1.80×10^{-7}	−6.75	−4.30	5.00×10^{-5}	4.35
				2.41×10^{-7}	−6.62	−4.19	6.43×10^{-5}	
				4.39×10^{-7}	−6.36	−3.93	1.17×10^{-4}	
				1.10×10^{-7}	−6.96	−4.53	2.95×10^{-5}	
				3.05×10^{-8}	−7.52	−5.09	8.14×10^{-6}	
4	−2.9064	−5.4000	2.4936	8.47×10^{-7}	−6.07	−3.64	2.26×10^{-4}	20.73
				5.36×10^{-7}	−6.27	−3.84	1.43×10^{-4}	
				5.18×10^{-8}	−2.06	−1.32	1.38×10^{-5}	
				3.84×10^{-7}	−6.42	−3.92	1.20×10^{-4}	
				5.09×10^{-7}	−6.29	−3.80	1.58×10^{-4}	
				1.02×10^{-6}	−5.99	−3.50	3.20×10^{-4}	
				4.45×10^{-7}	−6.35	−3.86	1.39×10^{-4}	
5	−2.8090	−5.3650	2.5560	7.77×10^{-7}	−6.11	−3.62	2.43×10^{-4}	19.83
				3.02×10^{-6}	−5.52	−3.03	9.42×10^{-4}	
				7.62×10^{-7}	−6.12	−3.62	2.38×10^{-4}	
				1.74×10^{-7}	−6.76	−4.20	6.25×10^{-5}	
				1.16×10^{-6}	−5.94	−3.38	4.18×10^{-4}	
6	−2.6190	−5.4030	2.7840	1.87×10^{-7}	−6.73	−4.17	6.74×10^{-5}	16.85
				2.78×10^{-6}	−5.56	−3.00	1.00×10^{-3}	
				1.01×10^{-6}	−6.00	−3.44	3.63×10^{-4}	
7	−2.4300	−5.5850	3.1550	6.10×10^{-7}	−6.21	−3.43	3.72×10^{-4}	41.35
				1.71×10^{-7}	−6.77	−3.98	1.04×10^{-4}	
				3.17×10^{-7}	−6.50	−3.71	1.93×10^{-4}	
				7.62×10^{-8}	−7.12	−3.96	1.09×10^{-4}	
8	−2.4990	−4.9720	2.4730	4.57×10^{-7}	−6.34	−3.18	6.55×10^{-4}	10.74
				4.27×10^{-7}	−6.37	−3.21	6.10×10^{-4}	
				8.47×10^{-7}	−6.07	−2.92	1.21×10^{-3}	
9	−2.7310	−5.5470	2.8160	3.29×10^{-7}	−6.48	−4.01	9.78×10^{-5}	7.90
				4.30×10^{-7}	−6.37	−3.89	1.28×10^{-4}	
				5.18×10^{-7}	−6.29	−3.81	1.54×10^{-4}	
				2.13×10^{-7}	−6.67	−3.85	1.40×10^{-4}	
				9.14×10^{-8}	−7.04	−4.22	5.97×10^{-5}	

Table 3. Cont.

Polygon #	Log K_{pump} (m/s)	Log K_{lab} (m/s)	$K_{diff} = \text{Log } K_{pump} - \text{Log } K_{lab}$ (m/s)	Test Hole K_{lab} (m/s)	Log K_{lab} (m/s)	Log $K_{model} = K_{diff} + \text{Log } K_{lab}$ (m/s)	K_{model} (m/s)	Geometric Mean K (m/day)
10	−2.6600	−5.2430	2.5830	2.13×10^{-7}	−6.67	−4.09	8.17×10^{-5}	22.75
				1.39×10^{-6}	−5.86	−3.27	5.33×10^{-4}	
				4.54×10^{-7}	−6.34	−3.76	1.74×10^{-4}	
				2.14×10^{-6}	−5.67	−3.09	8.17×10^{-4}	
				5.36×10^{-7}	−6.27	−3.69	2.05×10^{-4}	
11	−2.9010	−5.5050	2.6040	9.14×10^{-8}	−7.04	−4.43	3.66×10^{-5}	6.14
				3.05×10^{-8}	−7.52	−4.91	1.23×10^{-5}	
				3.81×10^{-7}	−6.42	−3.82	1.53×10^{-4}	
				9.45×10^{-7}	−6.02	−3.42	3.81×10^{-4}	
				1.74×10^{-7}	−6.76	−4.16	6.98×10^{-5}	
12	−2.9930	−5.6510	2.6580	2.33×10^{-6}	−5.63	−2.97	1.06×10^{-3}	40.56
				4.57×10^{-7}	−6.34	−3.68	2.08×10^{-4}	
13	−2.7770	−5.4480	2.6710	2.34×10^{-6}	−5.63	−2.96	1.10×10^{-3}	34.24
				7.01×10^{-7}	−6.15	−3.48	3.29×10^{-4}	
				2.86×10^{-7}	−6.54	−3.87	1.34×10^{-4}	
				5.64×10^{-6}	−5.25	−2.58	2.64×10^{-3}	
14	−2.9000	−5.3100	2.4100	1.65×10^{-7}	−6.78	−4.11	7.71×10^{-5}	39.24
				6.10×10^{-7}	−6.21	−3.80	1.57×10^{-4}	
				5.15×10^{-6}	−5.29	−2.88	1.32×10^{-3}	
15	−1.8210	−6.0140	4.1930	3.05×10^{-8}	−7.52	−3.32	4.75×10^{-4}	65.05
				7.62×10^{-8}	−7.12	−2.93	1.19×10^{-3}	
16	−2.4260	−6.1510	3.7250	3.05×10^{-8}	−7.52	−3.79	1.62×10^{-4}	85.59
				3.90×10^{-6}	−5.41	−1.68	2.07×10^{-2}	
				1.34×10^{-7}	−6.87	−3.15	7.13×10^{-4}	
				7.62×10^{-8}	−7.12	−3.39	4.05×10^{-4}	
17	−2.9180	−5.3760	2.4580	5.97×10^{-7}	−6.22	−3.77	1.71×10^{-4}	14.80

3. Results and Discussion

Wells are often drilled without prior information of the permeable/saturated hydrological repositories. Hydrogeological parameters such as porosity (Φ), formation factors (F), tortuosity (τ), and hydraulic conductivity (K) that are necessary for effective groundwater extraction and management are not all considered [77–79]. These pore properties also control fluid transmissibility in geologic units [80]. In the present study, pumping test values (K_{pump}) were significantly higher than laboratory values (K_{lab}) and hence, cannot be used to compute hydrological parameters because these values are not true representative as their physical properties were changed during the drilling process. To compute true representative values, a new methodology has been introduced those bridges hydraulic conductivity data with lab measurements. The difference (K_{diff}) between K_{lab} and K_{pump} was added to the individual laboratory conductivities, previously evaluated, and on this basis, new conductivities were obtained for the model, termed as “ K_{model} ”. The zones are made for the K_{model} values for the aquifer and are shown in Figure 7.

Fractional porosity (Φ) is a volumetric parameter and plays an important role in assessing the aquifer potential. It was calculated using Equation (3) developed by [81].

$$\Phi = 25.5 + 4.5 \ln K_h \quad (3)$$

The porosity of each polygon was estimated and is given in Table 4. The estimated values of porosity vary across the study area that represents the sandy aquifer. The interpreted porosity values range from 32 to 45% with an average of 38.5%. These values

reflect the presence of sand having variable grain sizes. Higher values indicated the fine sand or silty sand while the lower values represent the coarse sand which is also confirmed the lithological column of the already drilled water wells.

Table 4. Interpreted aquifer parameters based on VES and the estimated hydraulic parameters.

Polygon #	K (m/Day)	Φ (%)	Formation Factor (F)	Aquifer Resistivity (Ohm-m)	Aquifer Thickness (m)	Tortuosity	Transmissivity m ² /Day
1	12.11	36.72	6.71	28–52	78	15.7	944.89
2	23.67	39.74	5.77	26–48	57	15.1	1349.47
3	4.35	32.11	12.17	32–55	155	19.8	673.51
4	20.73	39.14	4.49	29–63	64	13.2	1326.43
5	19.83	38.94	4.52	34–69	105	13.3	2082.15
6	16.85	38.21	5.65	35–82	164	14.7	2764.09
7	41.35	42.25	5.14	31–69	139	14.7	5747.03
8	10.74	36.18	6.90	21–67	176	15.8	1891.04
9	7.90	34.80	7.43	26–71	172	16.1	1358.87
10	22.75	39.56	8.44	22–81	85	18.3	1934.02
11	6.14	33.66	12.23	29–88	178	20.3	1092.21
12	40.56	42.16	7.29	32–69	170	17.5	6894.43
13	34.24	41.40	7.60	25–66	167	17.7	5717.27
14	39.24	42.01	4.00	23–51	175	13.0	6866.78
15	65.05	44.29	4.70	28–48	101	14.4	6569.72
16	85.59	45.52	4.46	32–54	105	14.2	8986.72
17	14.80	37.63	8.59	33–64	183	18.0	2708.42

The precise and accurate measurement of the formation factor depends largely on the precise measurement of electrical conductivity, clay contents, and cementing factor of the water conductive layer [82]. Generally, an increasing trend is noted in the formation factor with an increase in cementing factor, decrease in porosity and clay contents. The formation factor is estimated by using well-known Archie's Equation (4).

$$F = a/\phi^m \quad (4)$$

where "a" is the tortuosity factor and "m" is the cementation exponent, and " ϕ " is porosity. The value of "a" and "m" depends on the site-specific lithology. In general m and a are equivalent to 2 and 1, respectively [61,83]. As per Archie [84] "m" varies from 1.7 to 3.0 but normally is 2.0. For the present study, a = 1 and the value of m ranged from 1.5 to 2.3. These dimensionless constants affect the geometric spread of formation factor and porosity. The mechanisms involving non-connectivity between pores or increase in pore communication are described by the cementation factor, such that m approaches unity when pore throats are closer to pore radius [85]. The computed values are given in Table 4. These values ranged from 4 to 12.2, showing a large variation in the texture of the aquifers.

Tortuosity is a geometric parameter of porous media that describes the interconnected pore spaces and relates with hydraulic and electrical properties [85–87]. It controls the flow of water in an aquifer and depends on the formation factor with aquifer porosity. Tortuosity can be estimated with the help of Equation (5) [88].

$$\tau = (F \phi)^{1/2} \quad (5)$$

Tortuosity calculated for 17 polygons that represent the area is presented in Table 4. This indicates that high tortuosity corresponds to low porosity and affects aquifer transmissibility and pore connectivity. The computed final values of hydraulic conductivity varied from 4.5 to 85.6 m/day affect the natural flow of fluids in the aquifer while tortuosity value ranges from 13 to 20.

Transmissivity is an important parameter in assessing the aquifer potential and can be computed by using Equation (6) [17,64]. It describes the capacity of the aquifer to transmit groundwater wholly in its entire saturated thickness [89] (Omeje et al., 2021). It can also be defined as the rate of flow of water through a vertical strip of the aquifer [90].

$$T = Kb \quad (6)$$

where K is hydraulic conductivity (m/day) and b is the thickness of the aquifer measured in meters. The thickness of the aquifer is estimated for each VES by using IXID software which is given in Table 4. The evaluated thickness of the aquifer varies from 57 to 183 m. The transmissivity values of the aquifer vary in a large range (674 to 8986 m²/day) due to strong contrast in the aquifer lithology. The very low transmissivity, hydraulic conductivity, and formation factor are associated with fine-grain sediments. These fine-grain sediments are mainly sand with silt/minor clay and comprise the aquifer of sandy plain zones.

Apparent resistivity ($\rho_a = \Delta V/I^* K$) computed in the field at different depths is an average value of various subsurface layers and does not represent the true electrical characteristics of the individual subsurface layer. Since resistivity values exhibit large variations with some repetition, the number of subsurface layers revealed by the resistivity survey do not often match with the results obtained by trial boring. Layers encountered by trial boring shall be greater in number than layers interpreted by resistivity survey. Apparent resistivity values are not a true representation of the subsurface lithology until they are matched with the theoretical master curves drawn manually or through computer modeling. The VES data collected at 50 probes were modeled by using the IXID Computer Software that gives the model interpretation of individual curves stating/reflecting the number of layers, their true resistivity values with thickness, and depth from the surface. From 50 points, some of the points are near the existing water well/test holes that were used for calibration purposes to correlate the true resistivities with subsurface permeable and impervious layers. These standardized values were applied to the rest of the probes and interpreted the subsurface lithologies. Subsurface geological material as depicted from resistivity modeling was composed of layers of sand, clay, and silt mixed with gravel/sand. The dominant subsurface encountered at all sites (given in Table 1) consists of sand containing fresh, saline, and brackish water. The sand formation containing freshwater indicated high resistivity values as compared to sand containing saline water. The lower resistivity values less than 20 ohm-m below the water table from comparatively the deeper horizon indicated the sand containing brackish water whereas the same range of values near the surface indicated the silt containing saline water. After drilling, the aquifer must be evaluated in order to determine the aquifer hydraulic properties. These parameters are evaluated with the help of pumping tests that help recommend the capacity of the pump as well as the depth of installation to improve the life and stabilization of the aquifer. The pumping test is conducted to examine the aquifer response, under controlled conditions, to the abstraction of water

The results of the pumping test are considered accurate and are used to evaluate the hydraulic properties. In this study, the hydraulic conductivity of rock samples collected at different depths from test holes was also available, but these values were lower than the conductivity obtained from the pumping test analysis due to the well-known factors that the samples obtained from different depths were disturbed and their physical properties (porosity, packing, grain orientation) also changed. To map the hydraulic conductivity laterally of the investigated area, the values of hydraulic conductivities evaluated from the pumping test with laboratory analysis were utilized by converting the area into 17 polygons where the pumping test was conducted. The final values of hydraulic conductivities were

estimated and are given in Table 3. The estimated hydraulic conductivities that represented the area falls in the range of 4.4 to 85.6 m/day. The highest value is interpreted at the junction of the Indus and Sutlej Rivers. This reflects the way they were deposited of the transported material in nature by rivers. Later, the values of transmissivity have been estimated by calculating the average thickness of the aquifer with the help of VES data for each polygon that ranged from 674 to 8986 m²/day. The transmissivity values evaluated for each polygon are shown in Table 4. Afterward, by using the already established relations having the same geological environments, the values of porosity, formation factor, and tortuosity were estimated of the whole investigated area. It is obvious from the results (Table 4) that the hydraulic conductivity increases with the increase in porosity indicating the high potential area. The higher values of the porosity are estimated towards the northern sides of the area where the Indus and Sutlej Rivers intersect each other due to the obvious reason those maximum sediments are deposited at these places.

4. Conclusions

A total of 50 vertical electrical soundings (VES) were analyzed and true resistivities with the thickness of individuals have been identified. The results showed that resistivity values range from 20 to 90 ohm-m with a minimum thickness of 57 m while the maximum thickness of 178 m of unconfined aquifer material consists of dominant sand containing fresh, marginally fresh, and brackish water. Further based on true resistivity values various aquifer regions of fresh, brackish, and saline water were differentiated. The lithology consists of silt/clay having resistivity <20 ohm-m representing saline water. Sand containing marginally fresh water and freshwater having resistivity 20–40 and 40–55 ohm-m, respectively. Whereas a mixture of sand and gravel containing freshwater having resistivity values ranged from 55–90 ohmmeters. Based on this standardization (Table 2), the water quality at different depths has been interpreted based on true resistivity values. This calibration shows the intermixing of resistivity values for subsurface layers, which cause overlapping of fresh–brackish and brackish–saline groundwater zones.

Hydraulic properties of the area were estimated by using the pumping test data, hydraulic conductivities estimated in the lab, VES data, and previously established regression equation. In the current study, the focus was to evaluate the hydraulic conductivity and afterward transmissivity, porosity, formation factor, and tortuosity based on the estimated value of K. The estimated hydraulic conductivity, transmissivity, porosity, formation factor, and tortuosity values of the aquifer range from 4.4 to 85.6 m/day, 674 to 8986 m²/day, 32 to 45 %, 4 to 12, and 13 to 20, respectively. Higher hydraulic conductivities were encountered in the southern portion of the area near the junction of the river as compared to the rest of the area. The porosity is also in an increasing trend. It is also concluded that the polygons representing aquifer having $T > 5700$ m²/day and $K > 40$ m/day, are considered excellent aquifer which can yield a large quantity of water. On the other hand, the polygons with $T < 1100$ m²/day and $K < 13$ m/day are considered comparatively low yield aquifer.

Author Contributions: Conceptualization, G.A. and Y.G.; methodology, G.A.; software, G.A., M.H.; validation, G.A., Y.S. and Y.G.; formal analysis, M.H., G.A.; investigation, G.A. and Y.G.; resources, Y.G. and Y.S.; data curation, Y.S. and M.H.; writing—original draft preparation, M.H. and Y.G.; writing—review and editing, G.A. and Y.S.; visualization, G.A.; supervision, Y.G.; project administration, Y.G.; funding acquisition, Y.G. All authors have read and agreed to the published version of the manuscript.

Funding: This research is financially supported by the Chinese Academy of Sciences President's International Fellowship Initiative (Grant No. 2021VCA0010) and the International Science & Technology Cooperation Program of China (2018YFE0100100).

Institutional Review Board Statement: Not applicable.

Informed Consent Statement: Not applicable.

Data Availability Statement: Not applicable.

Acknowledgments: The authors wish to acknowledge the Chinese Academy of Sciences President's International Fellowship Initiative and the International Science & Technology Cooperation Program of China financially supported the current research. The authors would like to greatly acknowledge the support extended by the Director (Hydrology) Of PCRWR. Special thanks of gratitude to the Director and Executive Director of China-Pakistan Joint Research Centre (CPJRC) on Earth Sciences for their encouragement, support during the entire period of research.

Conflicts of Interest: No conflict of interest.

References

1. Alam, U.; Sahota, P.; Jeffrey, P. Irrigation in the Indus basin: A history of unsustainability? *Water Supply* **2007**, *7*, 211–218. [CrossRef]
2. Watto, M.A. The Economics of Groundwater Irrigation in the Indus Basin, Pakistan: Tube-Well Adoption, Technical and Irrigation Water Efficiency and Optimal Allocation. Ph.D. Thesis, University of Western Australia, Perth, Australia, 2015.
3. Mondal, P.; Dalai, A.K. *Sustainable Utilization of Natural Resources*; CRC Press: Boca Raton, FL, USA, 2017. [CrossRef]
4. Yu, W.H.; Yang, Y.-C.; Savitsky, A.; Alford, D.; Brown, C. *The Indus Basin of Pakistan: The Impacts of Climate Risks on Water and Agriculture*; World Bank Publications: Herndon, VA, USA, 2013; Available online: <http://hdl.handle.net/10986/13834> (accessed on 10 January 2022).
5. Mukherjee, A. Overview of the groundwater of South Asia. In *Groundwater of South Asia*; Springer Science and Business Media LLC: Dordrecht, The Netherlands, 2018; pp. 3–20. Available online: https://link.springer.com/chapter/10.1007/978-981-10-3889-1_1 (accessed on 10 January 2022).
6. Bakhsh, A.; Awan, Q. Water issues in Pakistan and their remedies. In Proceedings of the National Symposium on Drought and Water Resources in Pakistan, Punjab, Pakistan, 16 March 2002; pp. 145–150.
7. Bakhsh, A.; Kanwar, R.S.; Pederson, C.; Bailey, T.B. N-Source Effects on Temporal Distribution of NO₃-N Leaching Losses to Subsurface Drainage Water. *Water Air Soil Pollut.* **2007**, *181*, 35–50. [CrossRef]
8. Saeed, M. *Skimming Wells*; Higher Education Commission: Islamabad, Pakistan, 2008.
9. Sikandar, P.; Christen, E.W. Geoelectrical Sounding for the Estimation of Hydraulic Conductivity of Alluvial Aquifers. *Water Resour. Manag.* **2012**, *26*, 1201–1215. [CrossRef]
10. Hasan, M.; Shang, Y.; Akhter, G.; Jin, W. Application of VES and ERT for delineation of fresh-saline interface in alluvial aquifers of Lower Bari Doab, Pakistan. *J. Appl. Geophys.* **2019**, *164*, 200–213. [CrossRef]
11. Greenman, D.; Swarzenski, W.; Bennett, G. *Ground-Water Hydrology of the Punjab Region of West Pakistan, with Emphasis on Problems Caused by Canal Irrigation*; WASID Bulletin 6; West Pakistan Water and Power Development Authority: Punjab, Pakistan, 1967. Available online: <https://pubs.er.usgs.gov/publication/wsp1608H> (accessed on 10 January 2022).
12. Ahmad, N. *Waterlogging and Salinity Problems in Pakistan*; Government of Pakistan, Scientific and Technological Research Division, Irrigation, Drainage and Flood Control Research Council: Islamabad, Pakistan, 1974. Available online: https://books.google.com.sg/books/about/Waterlogging_and_Salinity_Problems_in_Pa.html?id=HD5EAAAAYAAJ&redir_esc=y (accessed on 10 January 2022).
13. Alam, K. A groundwater flow model of the Lahore City and its surroundings. In Proceedings of the Regional Workshop on Artificial Groundwater Recharge, Quetta, Pakistan, 10–14 June 1996; pp. 10–14.
14. Mashadi, S.; Mohammad, A. Recharge the depleting aquifer of Lahore Metropolis. In Proceedings of the Regional Groundwater Management Seminar, Islamabad, Pakistan, 9–11 October 2000; pp. 209–220.
15. Qureshi, A.S.; Gill, M.A.; Sarwar, A. Sustainable groundwater management in Pakistan: Challenges and opportunities. *Irrig. Drain. J. Int. Comm. Irrig. Drain.* **2010**, *59*, 107–116. [CrossRef]
16. Soupios, P.M.; Kouli, M.; Vallianatos, F.; Vafidis, A.; Stavroulakis, G. Estimation of aquifer hydraulic parameters from surficial geophysical methods: A case study of Keritis Basin in Chania (Crete—Greece). *J. Hydrol.* **2007**, *338*, 122–131. [CrossRef]
17. Fetter, C. *Applied Hydrogeology*, 3rd ed.; University of Wisconsin-Oshkosh, Mc Millian College Publishing Company: New York, NY, USA, 1994.
18. Bowling, J.C.; Rodriguez, A.B.; Harry, D.L.; Zheng, C. Delineating Alluvial Aquifer Heterogeneity Using Resistivity and GPR Data. *Ground Water* **2005**, *43*, 890–903. [CrossRef] [PubMed]
19. Chowdhury, A.; Jha, M.K.; Chowdary, V.M. Delineation of groundwater recharge zones and identification of artificial recharge sites in West Medinipur district, West Bengal, using RS, GIS and MCDM techniques. *Environ. Earth Sci.* **2010**, *59*, 1209–1222. [CrossRef]
20. Lee, S.; Kim, Y.-S.; Oh, H.-J. Application of a weights-of-evidence method and GIS to regional groundwater productivity potential mapping. *J. Environ. Manag.* **2012**, *96*, 91–105. [CrossRef] [PubMed]
21. Nwachukwu, M.A.; Feng, H.; Achilike, K. Integrated study for automobile wastes management and environmentally friendly mechanic villages in the Imo River Basin, Nigeria. *Afr. J. Environ. Sci. Technol.* **2010**, *4*, 4.
22. Naghibi, S.A.; Pourghasemi, H.R.; Dixon, B. GIS-based groundwater potential mapping using boosted regression tree, classification and regression tree, and random forest machine learning models in Iran. *Environ. Monit. Assess.* **2016**, *188*, 44. [CrossRef] [PubMed]

23. Hasan, M.; Shang, Y.; Jin, W.; Akhter, G. Geophysical investigation of a weathered terrain for groundwater exploitation: A case study from Huidong County, China. *Explor. Geophys.* **2021**, *52*, 273–293. [CrossRef]
24. Akhtar, N.; Mislan, M.S.; I Syakir, M.; Anees, M.T.; Yusuff, M.S.M. Characterization of aquifer system using electrical resistivity tomography (ERT) and induced polarization (IP) techniques. *IOP Conf. Ser. Earth Environ. Sci.* **2021**, *880*, 012025. [CrossRef]
25. Bowling, J.C.; Harry, D.L.; Rodriguez, A.B.; Zheng, C. Integrated geophysical and geological investigation of a heterogeneous fluvial aquifer in Columbus Mississippi. *J. Appl. Geophys.* **2007**, *62*, 58–73. [CrossRef]
26. Iqbal, N.; Hossain, F.; Lee, H.; Akhter, G. Integrated groundwater resource management in Indus Basin using satellite gravimetry and physical modeling tools. *Environ. Monit. Assess.* **2017**, *189*, 128. [CrossRef] [PubMed]
27. Bhatti, S.A. *Analysis of Aquifer Characteristics and Probable Lowering of Water Levels in Bari Doab*; Wasid Publication No. 63; WAPDA: Lahore, Pakistan, 1969.
28. Akhter, G.; Ge, Y.; Iqbal, N.; Shang, Y.; Hasan, M. Appraisal of Remote Sensing Technology for Groundwater Resource Management Perspective in Indus Basin. *Sustainability* **2021**, *13*, 9686. [CrossRef]
29. Water and Power Development Authority (WAPDA). *Hydrogeological Data of Bari Doab (No. Vol.1, Pub. No. 27)*; Directorate General of Hydrogeology WAPDA: Lahore, Pakistan, 1980.
30. Kidwai, Z.D.; Alam, S. *The Geology of Bari Doab, West Pakistan (Bulletin#8)*; Water and Power Development Authority (WAPDA): Punjab, Pakistan, 1964.
31. Bennett, G.D.; Rehman, A.-U.; Sheikh, I.A.; Alr, S. Analysis of Aquifer Tests in the Punjab Region of West Pakistan. US Geological Survey: 1967. Available online: <https://pubs.er.usgs.gov/publication/wsp1608G> (accessed on 10 January 2022).
32. Store, H.; Storz, W.; Jacobs, F. Electrical resistivity tomography to investigate geological structures of the earth's upper crust. *Geophys. Prospect.* **2000**, *48*, 455–471. [CrossRef]
33. Kearey, P.; Brooks, M.; Hill, I. *An Introduction to Geophysical Exploration*; John Wiley & Sons: Hoboken, NJ, USA, 2002. ISBN 978-0-632-04929-5. Available online: https://faculty.ksu.edu.sa/sites/default/files/AN_INTRODUCTION_TO_GEOPHYSICAL_EXPLORATION_brooks_0_0.pdf (accessed on 10 January 2022).
34. Mondal, N.C.; Singh, V.P.; Ahmed, S. Delineating shallow saline groundwater zones from Southern India using geophysical indicators. *Environ. Monit. Assess.* **2012**, *185*, 4869–4886. [CrossRef]
35. Grygar, T.M.; Elznicová, J.; Tumová, Š.; Faměra, M.; Balogh, M.; Kiss, T. Floodplain architecture of an actively meandering river (the Ploučnice River, the Czech Republic) as revealed by the distribution of pollution and electrical resistivity tomography. *Geomorphology* **2016**, *254*, 41–56. [CrossRef]
36. Lashkaripour, G.R.; Ghafoori, M.; Dehghani, A. Electrical resistivity survey for predicting Samsor aquifer properties, Southeast Iran. In Proceedings of the Geophysical Research Abstracts European Geosciences Union, Vienna, Austria, 24–29 April 2005. Available online: <https://www.semanticscholar.org/paper/Electrical-resistivity-survey-for-predicting-Samsor-Lashkaripour-Ghafoori/54824cd84005ab12c3b7d10510ac697f2489626d> (accessed on 10 January 2022).
37. Oseji, J.; Asokhia, M.; Okolie, E. Determination of groundwater potential in obiaruku and environs using surface geoelectric sounding. *Environmentalist* **2006**, *26*, 301–308. [CrossRef]
38. Bussian, A.E. Electrical conductance in a porous medium. *Geophysics* **1983**, *48*, 1258–1268. [CrossRef]
39. Senthil, K.M.; Gnanasundar, D.; Elango, L. Geophysical studies in determining hydraulic characteristics of an alluvial aquifer. *J. Environ. Hydrol.* **2001**, *9*, 1–8.
40. Singh, K. Nonlinear estimation of aquifer parameters from surficial resistivity measurements. *Hydrol. Earth Syst. Sci. Discuss.* **2005**, *2*, 917–938.
41. Moreira, C.A.; Cavalheiro, M.L.D.; Pereira, A.M.; Caron, F. Relações entre condutividade hidráulica, transmissividade, condutância longitudinal e sólidos totais dissolvidos para o aquífero livre de Caçapava do Sul (RS), Brasil. *Eng. Sanit. Ambient.* **2012**, *17*, 193–202. [CrossRef]
42. Choo, H.; Kim, J.; Lee, W.; Lee, C. Relationship between hydraulic conductivity and formation factor of coarse-grained soils as a function of particle size. *J. Appl. Geophys.* **2016**, *127*, 91–101. [CrossRef]
43. Rosa, F.T.; Moreira, C.A.; Carrara, A.; dos Santos, S.F. Análise das relações entre resistividade elétrica, condutividade hidráulica e parâmetros físico-químicos para o Aquífero Livre da Região de Corumbataí (SP). *Águas Subterrâneas* **2017**, *31*, 384–392. [CrossRef]
44. Hasan, M.; Shang, Y.; Akhter, G.; Khan, M. Geophysical Investigation of Fresh-Saline Water Interface: A Case Study from South Punjab, Pakistan. *Ground Water* **2017**, *55*, 841–856. [CrossRef] [PubMed]
45. Dhakate, R.; Chowdhary, D.K.; Rao, V.V.S.G.; Tiwary, R.K.; Sinha, A. Geophysical and geomorphological approach for locating groundwater potential zones in Sukinda chromite mining area. *Environ. Earth Sci.* **2012**, *66*, 2311–2325. [CrossRef]
46. Gao, Q.; Shang, Y.; Hasan, M.; Jin, W.; Yang, P. Evaluation of a Weathered Rock Aquifer Using ERT Method in South Guangdong, China. *Water* **2018**, *10*, 293. [CrossRef]
47. Loke, M.; Barker, R. Rapid least-squares inversion of apparent resistivity pseudosections by a quasi-Newton method1. *Geophys. Prospect.* **1996**, *44*, 131–152. [CrossRef]
48. Robinson, E.S. *Basic Exploration Geophysics*; John Wiley & Sons: New York, NY, USA, 1988.
49. Rucker, D.; Noonan, G.E.; Greenwood, W.J. Electrical resistivity in support of geological mapping along the Panama Canal. *Eng. Geol.* **2011**, *117*, 121–133. [CrossRef]
50. Balasubramanian, A.; Sharma, K.; SASTRI, J.V. Geoelectrical and hydrogeochemical evaluation of coastal aquifers of Tambraparni basin, Tamil Nadu. *Geophys. Res. Bull.* **1985**, *23*, 203–209.

51. Devaraj, N.; Chidambaram, S.; Panda, B.; Thivya, C.; Thilagavathi, R.; Ganesh, N. Geo-electrical approach to determine the lithological contact and groundwater quality along the KT boundary of Tamilnadu, India. *Model. Earth Syst. Environ.* **2018**, *4*, 269–279. [CrossRef]
52. Hussain, Y.; Ullah, S.F.; Akhter, G.; Aslam, A.Q. Groundwater quality evaluation by electrical resistivity method for optimized tubewell site selection in an ago-stressed Thal Doab Aquifer in Pakistan. *Model. Earth Syst. Environ.* **2017**, *3*, 15. [CrossRef]
53. Sonkamble, S. Electrical resistivity and hydrochemical indicators distinguishing chemical characteristics of subsurface pollution at Cuddalore coast, Tamil Nadu. *J. Geol. Soc. India* **2014**, *83*, 535–548. [CrossRef]
54. Adepelumi, A.A.; Ako, B.D.; Ajayi, T.R.; Afolabi, O.; Omotoso, E.J. Delineation of saltwater intrusion into the freshwater aquifer of Lekki Peninsula, Lagos, Nigeria. *Environ. Earth Sci.* **2009**, *56*, 927–933. [CrossRef]
55. Batayneh, A.T. Use of electrical resistivity methods for detecting subsurface fresh and saline water and delineating their interfacial configuration: A case study of the eastern Dead Sea coastal aquifers, Jordan. *Appl. Hydrogeol.* **2006**, *14*, 1277–1283. [CrossRef]
56. Suprapti, A.; Pongmanda, S. Estimation of aquifer parameters using pumping tests: Case study of hotel Makassar paradise. *IOP Conf. Ser. Earth Environ. Sci.* **2020**, *419*, 012118. [CrossRef]
57. Freeze, R.A.; Cherry, J.A. *Groundwater*; Prentice-Hall, Inc.: Englewood Cliffs, NJ, USA, 1979.
58. Akhter, G.; Hasan, M. Determination of aquifer parameters using geoelectrical sounding and pumping test data in Khanewal District, Pakistan. *Open Geosci.* **2016**, *8*, 630–638. [CrossRef]
59. Lesmes, D.P.; Friedman, S.P. *Relationships between the Electrical and Hydrogeological Properties of Rocks and Soils*; Springer Science and Business Media LLC: Dordrecht, The Netherlands, 2005; pp. 87–128.
60. Kouamé, I.K.; Douagui, A.G.; Bouatrin, D.K.; Kouadio, S.K.A.; Savané, I. Assessing the hydrodynamic properties of the fissured layer of granitoid aquifers in the Tchologo Region (Northern Côte d’Ivoire). *Heliyon* **2021**, *7*, 07620. [CrossRef] [PubMed]
61. Heigold, P.C.; Gilkeson, R.H.; Cartwright, K.; Reed, P.C. Aquifer Transmissivity from Surficial Electrical Methods. *Ground Water* **1979**, *17*, 338–345. [CrossRef]
62. Chenini, I.; Rafini, S.; Ben Mammou, A. A Simple Method to Estimate Transmissibility and Storativity of Aquifer Using Specific Capacity of Wells. *J. Appl. Sci.* **2008**, *8*, 2640–2643. [CrossRef]
63. Olatunji, S.; Musa, A. Estimation of Aquifer Hydraulic Characteristics from Surface Geoelectrical Methods: Case Study of the Rima Basin, Northwestern Nigeria. *Arab. J. Sci. Eng.* **2014**, *39*, 5475–5487. [CrossRef]
64. Okiongbo, K.S.; Mebine, P. Estimation of aquifer hydraulic parameters from geoelectrical method—A case study of Yenagoa and environs, Southern Nigeria. *Arab. J. Geosci.* **2014**, *8*, 6085–6093. [CrossRef]
65. Khalilidermani, M.; Knez, D.; Zamani, M.A.M. Empirical Correlations between the Hydraulic Properties Obtained from the Geoelectrical Methods and Water Well Data of Arak Aquifer. *Energies* **2021**, *14*, 5415. [CrossRef]
66. Türkkan, G.E.; Korkmaz, S. Relationship between hydraulic and geoelectrical parameters for alluvial aquifers in Bursa, Turkey—A case study. *Arab. J. Geosci.* **2021**, *14*, 2221. [CrossRef]
67. Water and Power Development Authority (WAPDA). *Hydrogeological Data of Bari Doab (Vol-II, Directorate General of Hydrogeology WAPDA)*; WAPDA: Lahore, Pakistan, 1982.
68. Shahid, M.D. Hydraulic Conductivity contouring by the analysis of aquifer tests and lithologic logs in Bari Doab area. *Bull. Pak. Counc. Res. Water Resour.* **1990**, *20*, 1.
69. Ahmad, Z. Numerical Ground water modelling of Rechna Doab flow system. In Proceedings of the Conference PCRWR, Islamabad, Pakistan, 6–9 December 2000.
70. Ahmad, Z. *Prickett and Lonquist Finite Difference Basic Aquifer Simulation Program for Wet and Dry Season, 2nd Golden Software, Version 5*; Department of Geological Sciences, University of Kentucky: Lexington, KY, USA, 1992.
71. Thiessen, A.H. Precipitation average for large areas. *Mon. Wea. Rev.* **1911**, *39*, 1082–1084. [CrossRef]
72. Rhynsburger, D. Analytic Delineation of Thiessen Polygons. *Geogr. Anal.* **1973**, *5*, 133–144. [CrossRef]
73. Mujtaba, G. Conjunctive Use of Geographic Information System (GIS) and 3-D Numerical Models (FEFLOW) to Characterize the Groundwater Flow Regimes of the Lower Thal Doab, Punjab, Pakistan. Ph.D. Thesis, Quaid-i-Azam University, Islamabad, Pakistan, 2013.
74. Hölting, B.; Coldewey, W.G. *Hydrogeology*; Springer: Berlin/Heidelberg, Germany, 2019; 24p.
75. Domenico, P.A.; Schwartz, F.W. *Physical and Chemical Hydrogeology*; John Wiley & Sons: New York, NY, USA, 1990.
76. Todd, D.K. *Groundwater Hydrology*, 3rd ed.; John Wiley & Sons: Hoboken, NJ, USA, 2015; p. 93. ISBN 978-0-471-05937-0. Available online: <https://www.wiley.com/en-ie/Groundwater+Hydrology,+3rd+Edition-p-9780471059370> (accessed on 10 January 2022).
77. Martínez, A.G.; Takahashi, K.; Núñez, E.; Silva, Y.; Trasmonte, G.; Mosquera, K.; Lagos, P. A multi-institutional and interdisciplinary approach to the assessment of vulnerability and adaptation to climate change in the Peruvian Central Andes: Problems and prospects. *Adv. Geosci.* **2008**, *14*, 257–260. [CrossRef]
78. Ebong, E.; Akpan, A.E.; Onwuegbuche, A.A. Estimation of geohydraulic parameters from fractured shales and sandstone aquifers of Abi (Nigeria) using electrical resistivity and hydrogeologic measurements. *J. Afr. Earth Sci.* **2014**, *96*, 99–109. [CrossRef]
79. Akpan, A.E.; Ugbaja, A.N.; George, N.J. Integrated geophysical, geochemical, and hydrogeological investigation of shallow groundwater resources in parts of the Ikom-Mamfe Embayment and the adjoining areas in Cross River State, Nigeria. *Environ. Earth Sci.* **2013**, *70*, 1435–1456. [CrossRef]
80. George, N.J.; Ibuot, J.C.; Obiora, D.N. Geoelectrohydraulic parameters of shallow sandy aquifer in Itu, Akwa Ibom State (Nigeria) using geoelectric and hydrogeological measurements. *J. Afr. Earth Sci.* **2015**, *110*, 52–63. [CrossRef]

81. Marotz, G. Technische Grundlageneiner Wasserspeicherung Imm Natürlichen Untergrund Habilitationsschrift. Ph.D. Thesis, Universität Stuttgart, Stuttgart, Germany, 1968.
82. Khalili, M.; Brissette, F.; Leconte, R. Stochastic multi-site generation of daily weather data. *Stoch. Hydrol. Hydraul.* **2009**, *23*, 837–849. [[CrossRef](#)]
83. Worthington, P.F. The uses and abuses of the Archie equations, 1: The formation factor-porosity relationship. *J. Appl. Geophys.* **1993**, *30*, 215–228. [[CrossRef](#)]
84. Archie, G.E. Classification of carbonate reservoir rocks and petrophysical considerations. *Aapg Bull.* **1952**, *36*, 278–298.
85. Aleke, C.G.; Ibuot, J.C.; Obiora, D.N. Application of electrical resistivity method in estimating geohydraulic properties of a sandy hydrolithofacies: A case study of Ajali Sandstone in Ninth Mile, Enugu State, Nigeria. *Arab. J. Geosci.* **2018**, *11*, 322. [[CrossRef](#)]
86. Clennell, M.B. Tortuosity: A guide through the maze. *Geol. Soc. Lond. Spec. Publ.* **1997**, *122*, 299–344. [[CrossRef](#)]
87. Matyka, M.; Khalili, A.; Koza, Z. Tortuosity-porosity relation in porous media flow. *Phys. Rev. E* **2008**, *78*, 026306. [[CrossRef](#)] [[PubMed](#)]
88. The Netherland Organization. *Geophysical Well Logging for Geohydrological Purposes in Unconsolidated Formations*; Groundwater Survey TNO; The Netherlands Organisation for Applied Scientific Research: Delft, The Netherlands, 1976.
89. Omeje, E.T.; Ugbor, D.O.; Ibuot, J.C.; Obiora, D.N. Assessment of groundwater repositories in Edem, Southeastern Nigeria, using vertical electrical sounding. *Arab. J. Geosci.* **2021**, *14*, 421. [[CrossRef](#)]
90. George, N.J.; Ibuot, J.C.; Ekanem, A.M.; George, A.M. Estimating the indices of inter-transmissibility magnitude of active surficial hydrogeologic units in Itu, Akwa Ibom State, southern Nigeria. *Arab. J. Geosci.* **2018**, *11*, 134. [[CrossRef](#)]